14th International Symposium on Turbulence and Shear Flow Phenomena (TSFP14)
Heidelberg, Germany, July 28–31, 2026

JET-TO-WAKE TRANSITION BEHIND ISOTROPIC POROUS SQUARE CYLINDERS

Chansoo Seol
Department of Mechanical System Design Engineering
Seoul National University of Science and Technology
232, Gongneung-ro, Nowon-gu, Seoul, 01811, South Korea
seemsujim@seoultech.ac.kr

Jihoon Jeong
Department of Mechanical System Design Engineering
Seoul National University of Science and Technology
232, Gongneung-ro, Nowon-gu, Seoul, 01811, South Korea
bamco4280@seoultech.ac.kr

Taehoon Kim
Department of Mechanical System Design Engineering
Seoul National University of Science and Technology
232, Gongneung-ro, Nowon-gu, Seoul, 01811, South Korea
tkim99@seoultech.ac.kr

ABSTRACT

This study presents an experimental investigation of bleeding flow characteristics in the wake of isotropic porous square cylinders, focusing on the influence of permeability and pore configuration over a broad range of Darcy numbers ($2.4 \times 10^{-5} < Da < 2.9 \times 10^{-3}$). The porous geometries were constructed using high-resolution 3D printing based on a periodic simple cubic lattice, which allows for independent control of permeability through the number of pores along the cylinder width, D, while keeping porosity fixed. Wind tunnel experiments were performed at high Reynolds number ($Re \approx 3.1 \times 10^4$) using planar particle image velocimetry (PIV) to characterize the downstream velocity field. The results show that both permeability and pore configuration strongly influence bleeding flow characteristics near the cylinder trailing edge. These behaviors are further interpreted using an analogy to multiple plane turbulent jets, revealing three distinct flow regions determined by the structural pattern of the bleeding flow. Self-similarity analysis confirms that the combined bleeding conforms to the classical plane-jet profile and the post-merge wake conforms to the canonical plane-wake profile. An analytical model for the merging length, based on the integration of the Darcy–Brinkman–Forchheimer model with a boundary-layer approximation, is shown to agree well with experimental measurements.

Introduction

Flow over and downstream of two-dimensional (2D) porous media has attracted considerable attention owing to its practical relevance in engineering and environmental contexts. Porous bluff bodies exhibit fundamentally different downstream flow structures compared with their solid counterparts, primarily because of the bleeding flow — the fluid that passes through the porous structure and is emitted from its surfaces. Bleeding occurs both longitudinally and laterally, and these two components interact to collectively alter the downstream wake (Yu *et al.*, 2010; Taddei *et al.*, 2016; Ledda *et al.*, 2018). In particular, longitudinal bleeding has been shown to reduce the size of recirculation bubbles, weaken shear-layer intensity, and shift the shear-layer merging point further downstream (Zong & Nepf, 2012; Tang *et al.*, 2019; Seol *et al.*, 2024).

Despite this additional complexity, the far wake of porous bodies retains the characteristics of a turbulent free-shear flow. Nicolai *et al.* (2020) and Bourhis & Buxton (2024) confirmed that the velocity deficit in the far wake of porous patches and disks exhibits self-similarity consistent with a canonical plane wake. However, these studies focused exclusively on the wake region where bleeding has already decayed, leaving the role of bleeding itself — how it evolves, interacts with the external flow, and ultimately transitions into a wake — comparatively unexplored.

A key insight was provided by Bradbury (1965), who showed that a plane jet issued into a co-flowing stream decays with downstream distance; when the centerline jet ve-

locity falls below the free-stream velocity, the jet disappears and the flow recovers as a wake. This jet-to-wake transition bears a resemblance to the downstream evolution of bleeding through porous media. Building on this analogy, Seol *et al.* (2026) conducted a detailed investigation of the bleeding flow characteristics behind isotropic porous square cylinders, using permeability as the primary control parameter. That study demonstrated that the longitudinal bleeding can be interpreted through an analogy with multiple plane turbulent jets, and identified three distinct flow regions — merging, combined, and wake — based on the structural evolution of the bleeding. Furthermore, an analytical framework was developed to predict the longitudinal extent of the merging region by integrating the streamwise momentum equation with the Darcy–Brinkman–Forchheimer (DBF) model under a boundary-layer approximation.

The present study takes the next step by examining whether this framework can be validated quantitatively through self-similarity analysis. Specifically, we test whether the combined bleeding conforms to the self-similar plane-jet profile and whether the post-merge wake conforms to the self-similar plane-wake profile, thereby providing a similarity-based description of the jet-to-wake transition behind porous square cylinders. High-resolution particle image velocimetry (PIV) measurements are performed over a wide range of Darcy numbers ($2.4\times10^{-5} < Da < 2.9\times10^{-3}$) at $Re \sim O(10^4)$.

Experiments

The porous cylinders used in this study were designed based on a simple cubic lattice structure, characterized by a unit cell length d_1 and a strut width d_2 (see figure 1). The porosity of this structure, $\Phi = (1-2d_2/d_1)^2(1+4d_2/d_1)$, depends solely on the ratio d_2/d_1. A key feature of this design is that permeability K can be varied independently of porosity by changing d_1 while keeping d_2/d_1 constant. Three porosities ($\Phi = 0.7$, 0.8 and 0.9) were tested, each with five unit-cell sizes, yielding 15 porous configurations that span $2.4\times10^{-5} < Da < 2.9\times10^{-3}$. All models were fabricated using high-resolution stereolithography (SLA) 3D printing. The cylinder width was $D = 40$ mm (or 42 mm) with a spanwise length of 320 mm.

Permeability was determined from pressure drop measurements conducted in an open-loop acrylic pipe (length 3.5 m, inner diameter 65 mm). Porous disks replicating the internal lattice geometry were fabricated with thicknesses ranging from 20 to 60 mm. The permeability K was estimated by fitting the pressure drop–superficial velocity data to the Forchheimer equation.

PIV measurements were carried out in an open-loop wind tunnel at Seoul National University of Science and Technology, with a $0.35\times0.35\times2.0$ m test section. All measurements were performed at a free-stream velocity of 11.5 m/s ($Re \approx 3.1\times10^4$). Two 12 MP cameras with 105 mm lenses were positioned at adjacent downstream stations, yielding a combined field of view of approximately $6D\times3D$. Further details on the experimental procedures can be found in Seol *et al.* (2023) and Seol *et al.* (2024).

Results

Figure 2(*a*) presents the lateral profiles of the mean longitudinal velocity, $\langle u\rangle/U_e$, at several downstream positions for selected porous cases, illustrating the structural evolution of longitudinal bleeding. For cases with larger pores and higher permeability (e.g. C4 and C5), multiple parallel jets emerge from individual lattice pores and gradually merge downstream into a single jet-like structure that spreads and decays. In contrast, for smaller-pore cases (e.g. A1 and B2), the velocity profiles at $x/D = 1.5$ already resemble a single jet, indicating rapid merging immediately behind the cylinder. These observations are further influenced by whether the number of pores across the cylinder width is odd or even, which determines the presence or absence of a central jet along the symmetry plane.

Table 1. Parameters for the structured porous square cylinders. ϕ: porosity; d_1: length of the unit cell; d_2: strut width; L_m: merging length; Da: Darcy number.

Case	Φ	d_1 (mm)	d_2 (mm)	L_m/D	Da ($\times10^{-4}$)
S	0	–	–	–	–
A1	0.7	2.0	0.36	0.23	0.24
A2	0.7	4.0	0.73	0.29	0.64
A3	0.7	6.0	1.09	0.36	0.97
A4	0.7	8.0	1.45	0.66	2.03
A5	0.7	10.0	1.82	0.99	4.07
B1	0.8	2.0	0.29	0.49	0.58
B2	0.8	4.0	0.57	0.39	1.39
B3	0.8	6.0	0.86	0.59	2.17
B4	0.8	8.0	1.15	0.82	4.17
B5	0.8	10.0	1.44	1.35	8.62
C1	0.9	2.0	0.20	0.34	1.09
C2	0.9	4.0	0.39	0.65	2.30
C3	0.9	6.0	0.59	1.14	7.16
C4	0.9	8.0	0.78	1.93	16.8
C5	0.9	10.0	0.98	2.29	28.6

Based on these observations, the downstream flow is divided into three distinct regions, as illustrated schematically in figure 2(*b*). The merging region, situated nearest to the cylinder, is where individual bleeding jets interact and coalesce. The combined region follows, where the merged jets behave as a single structure that progressively decays through interaction with the surrounding shear layers. The wake region is located downstream of the combined region, where the bleeding has fully dissipated and the flow recovers as a conventional wake. The boundaries of these regions are defined by the merging length L_m (the streamwise location of the combined point) and the combined-region length L_c (the location where the shear layers merge). This framework, originally proposed by Seol *et al.* (2026), provides a systematic basis for interpreting the complex evolution of bleeding flows behind porous bluff bodies.

The three-region framework naturally suggests that the combined bleeding and the post-merge wake may each conform to classical free-shear-flow similarity solutions. We test this hypothesis by examining the self-similar characteristics at two stages.

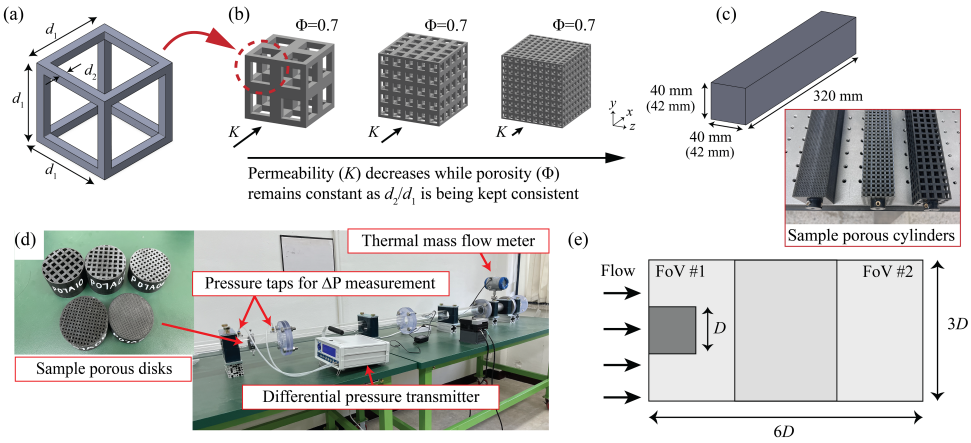

Figure 1. (a) Simple cubic lattice structure as a base porous structure; (b) schematic illustration of decoupling process of permeability from porosity; (c) examples of the current porous square cylinder; (d) experimental setup of the permeability measurement and its sample porous disks; (e) schematic representation of the PIV measurements

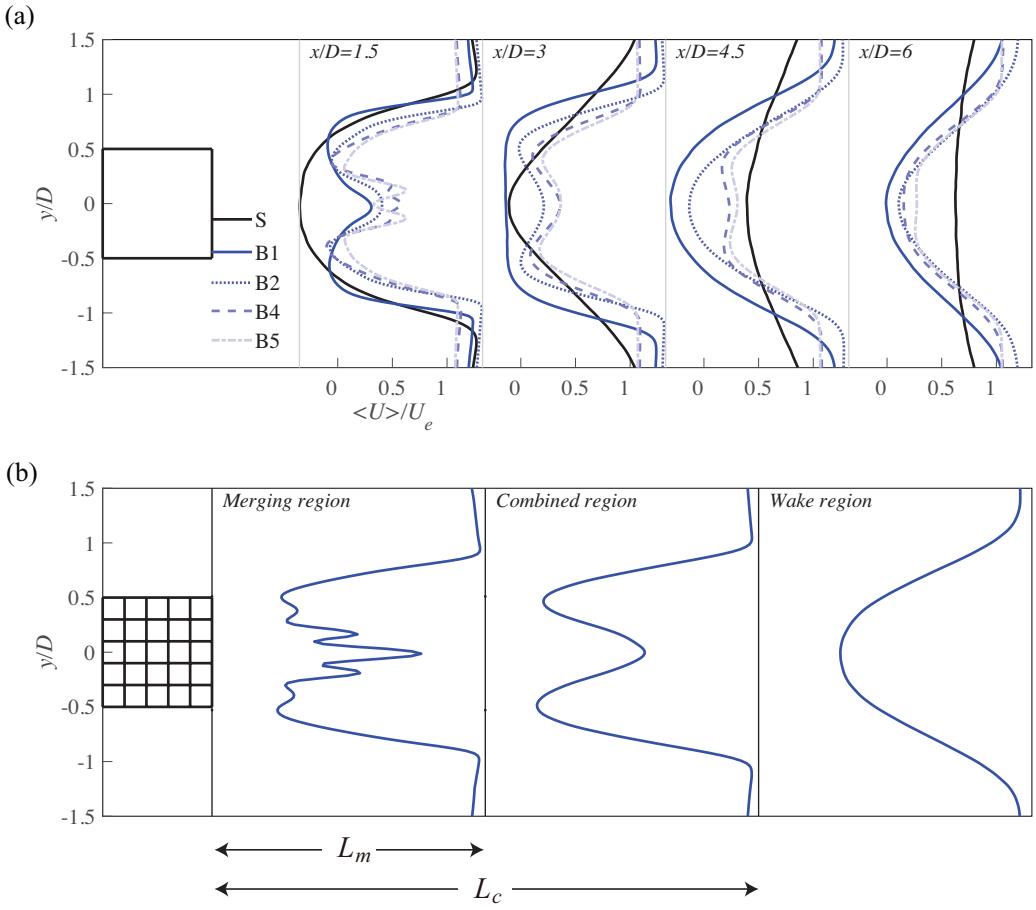

Figure 2. (a) Evolution of the longitudinal velocity profiles at multiple downstream positions ($x/D = 1.5$, 3, 4.5, and 6) for cases S, A1, B2, C4, and C5, corresponding to increasing Da. (b) Schematic illustration of the development of longitudinal bleeding jets, interacting with surrounding shear layers. The diagram highlights the merging, combined, and wake regions for the odd pore configuration.

In the combined region, the jet velocity $\langle u \rangle_j = \langle u \rangle - U_m$ is defined by subtracting the local minimum velocity U_m from the mean velocity, isolating the bleeding contribution from the surrounding base flow. Here, U_m serves as the reference velocity, analogous to the co-flow velocity in the classical plane-jet formulation (Bradbury, 1965; Pope, 2000). When scaled by the centerline jet velocity $U_{j,o}$ and the jet half-width δ_j, the lateral profiles at different streamwise locations within the combined region collapse onto a single curve for all 15 porous configurations, regardless of permeability and pore configuration. The collapsed profiles are well described by the classical plane-jet similarity form, $g(\eta) = \mathrm{sech}^2(\alpha_j \eta)$, where $\eta = y/\delta_j$. The fitted shape parameter is found to be approximately equal to the canonical value for a plane jet across all Darcy numbers inves-

tigated. This result confirms that, once the individual bleedings have merged, the combined bleeding possesses plane-jet self-similarity in the presence of an external co-flow. The absence of lateral jet spreading does not contradict the plane-jet analogy; rather, it is a natural consequence of the confining external stream, consistent with the findings of Bradbury (1965).

In the wake region, we examine whether the post-merge flow conforms to the self-similar plane-wake profile. The velocity deficit $\Delta\langle u\rangle = U_e - \langle u\rangle$ is scaled by the maximum deficit ΔU_o and the half-deficit width δ_w. For all cases in which the wake region is identified within the present field of view, the scaled deficit profiles are well described by the canonical Gaussian form, $f(\eta) = \exp(-\alpha_w \eta^2)$, with the shape parameter remaining close to the plane-wake value (Pope, 2000). It should be noted that, for several high-permeability cases, the shear-layer merge point L_c is not captured within the present field of view; these cases are therefore excluded from the wake analysis. The merge point $L_c + D$ serves as the reference position for the collapse of the wake profiles.

The findings from both stages indicate that these results support a similarity-based description of the downstream flow structure: the bleeding stage conforms to plane-jet self-similarity, and the post-merge stage conforms to plane-wake self-similarity. The self-similar functional forms — sech^2 for the jet and Gaussian for the wake — remain invariant across the range of Darcy numbers investigated, indicating that permeability governs the decay rate of the characteristic scales but does not alter the underlying self-similar structure.

To predict the longitudinal extent of the merging region, we developed an analytical model by integrating the streamwise momentum equation with the DBF model under a boundary-layer approximation. Along the lateral center ($y/D = 0$), the DBF model captures the macroscopic resistance of the porous medium in the near-wake region, while the boundary-layer equation governs the lateral diffusion in the combined region. The merging length L_m, defined as the streamwise position of the combined point, serves as the boundary between these two regimes. With appropriate scaling and simplifications valid at high Reynolds number, the model yields

$$L_m \sim \frac{7\sqrt{K}}{\sqrt{\Phi}} \ln\left[\frac{\Phi^2 U_e^2}{10D} \log\left(\frac{1}{2\sqrt{Da}}\right)\right] \qquad (1)$$

Figure 3 presents the merging length L_m/D as a function of Da, comparing the analytical model with experimental data. The model captures the overall log–log trend, with L_m increasing systematically with Da, consistent with the observation that higher permeability shifts the combined point farther downstream. The effect of porosity and the lateral diffusion term $\partial\overline{u'v'}/\partial y$ at the combined point are examined by varying their values in the model, establishing upper and lower bounds. All experimental data fall within the predicted boundaries, supporting the robustness of the analytical model.

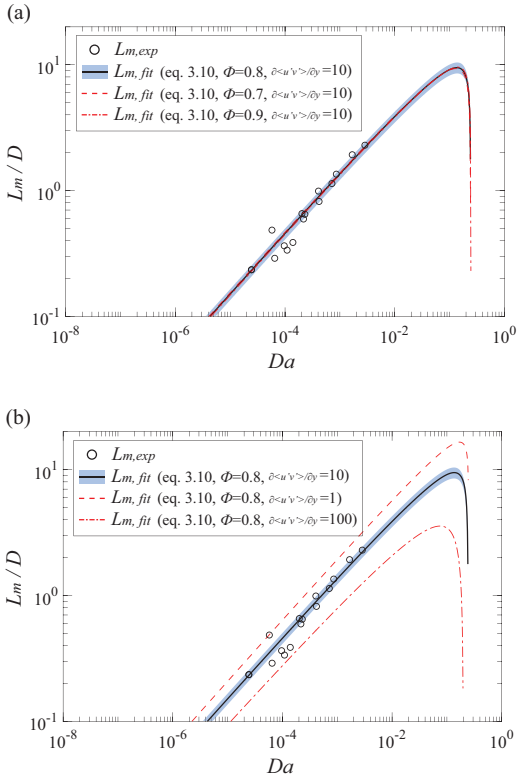

Figure 3. Merging region length L_m/D plotted against Da. Solid line: analytical prediction from (1) with $\Phi = 0.8$ and $\partial\langle u'v'\rangle/\partial y = 10$; symbols: experimental measurements. The blue shaded region indicates the 95 % confidence interval. (*a*) Sensitivity to porosity ($\Phi = 0.7$, 0.8 and 0.9). (*b*) Sensitivity to the lateral diffusion term $\partial\langle u'v'\rangle/\partial y$ at the combined point, evaluated for values of 1, 10 and 100.

Conclusion

This study investigated the structural characteristics of longitudinal bleeding flows behind isotropic porous square cylinders and their connection to the downstream wake structure, combining results from our recent studies (Seol *et al.*, 2026). The downstream flow structure is interpreted as a jet-to-wake transition: longitudinal bleedings emitted from individual lattice pores first merge, then behave collectively as a self-similar plane jet in the combined region, and ultimately decay into a self-similar plane wake once the shear layers have merged. Self-similarity analysis confirms that the combined bleeding conforms to the classical plane-jet profile and the post-merge wake conforms to the canonical plane-wake profile, with the functional forms remaining invariant across a wide range of Darcy numbers ($2.4\times10^{-5} < Da < 2.9\times10^{-3}$). An analytical model for the merging length, based on the integration of the DBF model with a boundary-layer approximation, is shown to agree well with experimental measurements. These findings provide a coherent similarity-based framework for interpreting the complex shear-layer dynamics downstream of porous bluff bodies through classical free-shear-flow theory. We note that the present results were obtained at a single Reynolds number; extending the analysis to different Re conditions and establishing the streamwise evolution of the characteristic scales remain as future work.

REFERENCES

Bourhis, M & Buxton, ORH 2024 Influence of freestream turbulence and porosity on porous disk-generated wakes. *Physical Review Fluids* **9** (12), 124501.

Bradbury, LJS 1965 The structure of a self-preserving turbulent plane jet. *Journal of Fluid Mechanics* **23** (1), 31–64.

Ledda, Pier Giuseppe, Siconolfi, Lorenzo, Viola, Francesco, Gallaire, François & Camarri, Simone 2018 Suppression of von kármán vortex streets past porous rectangular cylinders. *Physical Review Fluids* **3** (10), 103901.

Nicolai, Claudia, Taddei, Sonia, Manes, Costantino & Ganapathisubramani, Bharathram 2020 Wakes of wall-bounded turbulent flows past patches of circular cylinders. *Journal of Fluid Mechanics* **892**, A37.

Pope, Stephen B. 2000 *Turbulent Flows*. Cambridge University Press.

Seol, Chansoo, Hong, Jihye & Kim, Taehoon 2023 Flow around porous square cylinders with a periodic and scalable structure. *Experimental Thermal and Fluid Science* **144**, 110864.

Seol, Chansoo, Kim, Taewoo & Kim, Taehoon 2024 The effect of permeability on the flow structure of porous square cylinders. *Journal of Fluid Mechanics* **985**, A29.

Seol, Chansoo, Moon, Dohyun, Pathikonda, Gokul, Jee, Solkeun & Kim, Taehoon 2026 Bleeding flow characteristics downstream of isotropic porous square cylinders. *Journal of Fluid Mechanics* **1027**, A23.

Taddei, Sonia, Manes, Costantino & Ganapathisubramani, B 2016 Characterisation of drag and wake properties of canopy patches immersed in turbulent boundary layers. *Journal of Fluid Mechanics* **798**, 27–49.

Tang, Tingting, Yu, Peng, Shan, Xiaowen & Chen, Huisu 2019 The formation mechanism of recirculating wake for steady flow through and around arrays of cylinders. *Physics of Fluids* **31** (4).

Yu, P, Zeng, Y, Lee, TS, Bai, HX & Low, HT 2010 Wake structure for flow past and through a porous square cylinder. *International Journal of Heat and Fluid Flow* **31** (2), 141–153.

Zong, Lijun & Nepf, Heidi 2012 Vortex development behind a finite porous obstruction in a channel. *Journal of Fluid Mechanics* **691**, 368–391.